Polymer 51 (2010) 2565–2575

Contents lists available at ScienceDirect

Polymer

journal homepage: www.elsevier.com/locate/polymer

Estimation of thermal transitions in poly(ethylene naphthalate): Experiments and modeling using isoconversional methods

George Z. Papageorgiou*, Dimitris S. Achilias*, George P. Karayannidis

Laboratory of Organic Chemical Technology, Department of Chemistry, Aristotle University of Thessaloniki, 541 24 Thessaloniki, Greece

ARTICLE INFO

Article history:
Received 19 January 2010
Received in revised form
14 April 2010
Accepted 16 April 2010
Available online 24 April 2010

Keywords:
PEN
Crystallization kinetics
Isoconversional methods

ABSTRACT

Thermal transitions of PEN, such as the glass transition temperature and those occurring during isothermal or nonisothermal crystallization were investigated based on careful experiments and modeling with isoconversional methods. The latter was applied to DSC data to determine the effective activation energy for the glass transition in PEN. Using the same data and different thermal methods the dynamic fragility of PEN was evaluated. The Lauritzen–Hoffman (LH) parameters K_g and U^* were estimated using the secondary nucleation theory from both PLM and isothermal DSC after self-nucleation measurements. Regime II to I and III to II transition at about 253 °C and 243 °C were concluded. Elliptical-shaped hedrite-like morphology was observed above 253 °C. Finally, isoconversional analysis was applied to both melt and glass non-isothermal crystallization data and the combined set of activation energies was found to be described by the theoretical Vyazovkin–Sbirrazzuoli equation using a single set of LH parameters coming from PLM measurements.

1. Introduction

Poly(ethylene 2,6-naphthalene dicarboxylate), or poly(ethylene 2,6-naphthalate), or simply poly(ethylene naphthalate) (PEN) is a high performance transparent polyester that is attracting increasing commercial interest [1,2]. PEN has the naphthalene ring in the main chain instead of the benzene ring in the closely-related system of poly(ethylene terephthalate) (PET) [3]. The naphthalene ring provides greater rigidity to the polymer backbone than the benzene ring [4,5]. This imparts to PEN higher thermal properties, as well as enhances its mechanical properties, dimensional stability, and barrier properties, in comparison to PET. PEN has a higher glass transition temperature (T_g), 123 °C compared to approximately 80 °C for PET. Thus, among other plastics, PEN shares applications in the production of food containers, in particular plastic bottles, which can withstand the temperatures required for sterilization [6–8]. This high temperature resistance also means that PEN is useful as a substrate in the production of flexible printed circuits which can be soldered using conventional tin/lead alloys and in general PEN finds applications in microelectronics [9–13]. PEN is characterized by its inherent strength and dimensional stability, partially due to the presence of the co-joined benzene rings in the monomer [14]. The combination of these properties makes it useful for fibers and films, where low shrinkage and elongation properties are required [15].

Crystallization of PEN is very slower compared to that of PET, because the PEN chain is stiffer than that of PET [16–18]. PEN, like its close chemical relative, PET, can be quenched into an amorphous material, while it can be crystallized either by slow cooling from the melt, or by stretching between the glass transition temperature and the cold crystallization temperature [19–21]. The effect of storage and use conditions on the amorphous phase or even on the crystallized phase of PEN is of special importance [22–24].

A consequence of the exposure of a polymer at temperatures that approach the glass transition is the development of physical aging. Physical aging results in structural changes that increase the density and the brittleness of the material and change the electrical properties [25]. Physical aging or enthalpic relaxation is due to non-equilibrium state of the glass and as a result there is a thermodynamic driving force to reach equilibrium. Aging is particularly important from a commercial production perspective, since polymers like PEN are often injection or extruded molded, both processes involving a rapid quenching from the melt to ambient temperature [26,27]. This results in a non-equilibrium state that will exhibit physical aging. Therefore, if the product experiences service temperatures that approach the glass transition temperature, a time dependent change will occur in its properties outlined

* Corresponding authors.
E-mail addresses: gzpap@chem.auth.gr (G.Z. Papageorgiou), axilias@chem.auth.gr (D.S. Achilias).

0032-3861/$ – see front matter © 2010 Elsevier Ltd. All rights reserved.
doi:10.1016/j.polymer.2010.04.031

above [28]. The process of physical aging has been studied by a number of techniques, but in particular differential scanning calorimetry has been used extensively to measure the kinetics of the enthalpic relaxation process. Following storage at a temperature below the glass transition, an aged sample will exhibit an endotherm on the glass transition temperature, the area of which increases with the extent of aging.

An interesting question concerns the comparison of the temperature dependence of the relaxation times of the different observables [29]. In several studies it was found that the apparent activation energy at the glass transition coincides with enthalpy relaxation, viscous flow or dielectric relaxation. This finding has been recently validated by works in which the fragility of glass forming systems, as evaluated by thermal methods, was compared with the fragility obtained by viscoelastic or dielectric measurements [28,30,31]. It should be noted here that according to recent findings, the activation energy of enthalpy relaxation may change throughout the process and only for the later stages its value becomes comparable to that of the glass transition [32].

Crystallization kinetics of polymers is very important, since it determines the final degree of crystallinity and morphology of the polymers in the end products after processing [33]. In the case of polymer films or other polymeric parts, the degree of crystallinity and morphology determine mechanical properties, ultimate use temperature, dimensional stability, gas permeability and other important properties [34]. Like any phase transformation, crystallization, obeys the laws of thermodynamics that decide whether, under specific circumstances, crystals can exist or not [35]. However, the kinetics of the process determines whether crystallization takes place, and its speed [36]. Generally, studies on crystallization are limited to idealized and constant external conditions, resulting in a relatively easy theoretical analysis, since problems connected to cooling rates and thermal gradients within the specimens are avoided [37]. However, the study of crystallization in a continuously changing environment is of greater interest, since industrial processes proceed under non-isothermal conditions, that is the external conditions change continuously and this makes the treatment of non-isothermal crystallization more complex [38–41].

In this work, both the glass transition and the crystallization of PEN are analyzed. In particular the activation energy of the glass transition, fragility and relaxation times are studied applying conventional treatment of non-isothermal data [42–44]. Activation energy of the glass transition is also determined from data from non-isothermal experiments and then using an isoconversional method according to the procedure proposed by Vyazovkin et al. [42,43]. In case of crystallization, the isothermal process is studied by performing experiments in the DSC at various temperatures from 210 up to 260 °C following a self-nucleation method to approximate the spherulitic growth rates. Thus, the equilibrium melting point is determined. Also, true spherulitic growth rates were measured from polarized optical microscopy experiments at the same temperatures is discussed. Both series of kinetic data are used in the analysis following the secondary nucleation theory to obtain the nucleation parameter K_g and surface energies. The non-isothermal crystallization from the melt and the glassy state is also studied with respect to the activation energy.

2. Experimental

PEN was synthesized from dimethyl 2,6-naphthalate (DMN) and ethylene glycol (EG) by applying the two stage polycondensation method and by using catalyst tetrabutyl titanate (Tizor). Details of the synthesis procedure were described in a previous paper [2].

Intrinsic viscosity [η] measurements were performed using an Ubbelohde viscometer at 25 °C in a mixture of phenol and tetrachloroethane (60:40, w/w). The intrinsic viscosity of the sample was found to be 0.46 (dl g^{-1}).

DSC measurements were conducted by using a Perkin-Elmer Pyris Diamond DSC in a nitrogen atmosphere flow. A Perkin–Elmer Intracooler 2P cooling device was used to allow the DSC to achieve high and constant cooling rates.

Prior to study the glass transition of PEN, the semicrystalline sample of PEN was transformed into the amorphous state by heating to 300 °C at 20 °C/min and cooling to 25 °C in the DSC cell at 200 °C/min. The glass transition in the amorphous samples was studied by heating them to 150 °C, well above the glass transition temperature of PEN ($T_g = 123$ °C) and maintaining this temperature for 1 min. From previous studies [19] it had been found that crystallization of PEN may occur at temperatures above 160 °C. Therefore, the temperature and holding time were set equal to these values (i.e. 150 °C and 1 min) in order the sample to achieve equilibrium, quite above the T_g, but also assuring that crystallization during heating–holding–cooling scans is prevented. After that holding at 150 °C, the samples were cooled to 90 °C, that is significantly below T_g, at different cooling rates. Immediately after completion of the cooling segment, the samples were heated at a rate whose absolute value was equal to the rate of preceding cooling. The cooling/heating rates were as follows, 5, 10, 15, 20, and 25 °C/min. The sample mass was near 10 mg and each run was repeated at least twice in order to have repeatable results.

Isothermal crystallization experiments at various temperatures from 210 °C to 260 °C were performed after self-nucleation of the polyester sample. Self-nucleation measurements were performed in analogy to the procedure described by Fillon et al. [45] and Müller et al. [46,47]. The protocol used is very similar with that described by Müller et al. [47] and can be summarized as follows: a) melting of the sample at 300 °C for 5 min to erase any previous thermal history; b) cooling at 10 °C/min to 210 °C and crystallization for 12 min, to create a "standard" thermal history; c) partial melting by heating at 20 °C/min up to a "self-nucleation temperature", T_s which was 275 °C; d) thermal conditioning at T_s for 1 min. Depending on T_s, the crystalline polyester will be completely molten, only self-nucleated or self-nucleated and annealed. If T_s is sufficiently high, no self-nuclei or crystal fragments can remain (T_s Domain I – complete melting domain). At intermediate T_s values, the sample is almost completely molten, but some small crystal fragments or crystal memory effects remain, which can act as self-nuclei during a subsequent cooling from T_s (T_s Domain II-self – nucleation domain). Finally, if T_s is too low, the crystals will only be partially molten, and the remaining crystals will undergo annealing during the 5 min at T_s, while the molten crystals will be self-nucleated during the later cooling (T_s Domain III – self-nucleation and annealing domain); e) cooling scan from T_s at 200 °C/min to the crystallization temperature (T_c), where the effects of the previous thermal treatment will be reflected on isothermal crystallization; f) heating scan at 20 °C/min to 300 °C, where the effects of the thermal history will be apparent on the melting signal. Experiments were performed to check that the sample did not crystallize during the cooling to T_c and that a full crystallization exothermic peak was recorded at T_c. In heating scans after isothermal crystallization the standard heating rate was always 20 °C/min.

For non-isothermal crystallization from the melt the samples were heated to 300 °C, held there for 5 min and then cooled to 100 °C by the desired rate. Cooling scans were performed at rates 2.5, 3.75, 5, 6.25, 7.5, and 10 °C/min. For non-isothermal crystallization from the glass the samples were heated to 300 °C, held there for 5 min, cooled to 100 °C at 200 °C/min held for 1 min and then heated to 300 °C by the desired rate. Heating scans were performed at rates 2.5, 5, 7.5, 10, 15 and 20 °C/min. A fresh sample was used in each run.

A polarizing light microscope (Nikon, Optiphot-2) equipped with a Linkam THMS 600 heating stage, a Linkam TP 91 control unit and also a Jenoptic ProgRes C10Plus camera with the Capture Pro 2.1 software was used for PLM observations.

3. Results and discussion

3.1. Variation of the effective activation energy throughout the glass transition temperature

The variation of the effective activation energy (ΔE_x) through the glass transition can be determined as a function of the extent of conversion using isoconversional methods [42,43]. According to the Flynn, Wall, Ozawa (FWO) method [48,49] the value of ΔE_x at each value of conversion is calculated as shown in the following equation.

$$\left(\frac{\Delta E_X}{R}\right)_X = -\left(\frac{\mathrm{d}(\ln(\beta))}{\mathrm{d}(1/T)}\right)_X \quad (1)$$

where β is the cooling rate, R is the universal gas constant and T the temperature where the conversion X is attained.

ΔE_x can be measured upon cooling through the glass transition using the above equation as thermodynamic properties such as C_p exhibit a monotonic decrease upon transformation from an equilibrium liquid to a glass; however, when measured on heating, C_p often shows an overshoot near the glass transition and the size of the enthalpic overshoot is influenced by thermal history and the heating rate [44]. In order to estimate the effective activation energy through the glass transition region using an isoconversional analysis the conversion, X, has to be defined. The extent of conversion, X, needed for the computations is determined as the normalized heat capacity, C_p^N, that is determined from DSC scans as

$$C_p^N = \frac{(C_p - C_{pg})|_T}{(C_{pe} - C_{pg})|_T} \equiv X \quad (2)$$

where C_{pg} and C_{pe} refer to the glassy and the equilibrium (liquid) heat capacities, respectively. T_g is calculated from DSC measurements as the temperature where the step change in C_p^N attains half the value of the total change.

Note that this definition is the same with that used by Vyazovkin et al. [42,43] while opposite to that used by Badrinarayanan et al. [44,50] for evaluating cooling curves where $X = 0$ is taken to be the liquid and $X = 1$ is taken to be the glass.

Fig. 1 displays DSC data taken in the vicinity of T_g at different heating rates. By transforming DSC data to the normalized heat capacity, C_p^N vs T data sets similar to that shown in Fig. 2 are obtained.

Application of the FWO isoconversional method to the C_p^N vs T data yields the effective activation energy at different degrees of X. Typical plots of $\ln(\beta)$ vs $1/T$ at different Xs appear in Fig. 3. It should be noted here that in Fig. 3 only heating rates 10, 15, 20 and 25 °C/min were included since it was observed that using the whole range i. e. from 5 to 25 °C/min a curvature appeared at values of X greater than 60%. Then, the estimated values of ΔE_x using the two different heating rate regimes are plotted as a function of X in Fig. 4. When employing the whole heating range the values increased with X, while when using 10–25 °C/min the dependency demonstrated a decrease with the extent of conversion from the glassy to the liquid state that is in agreement with literature findings [42,43]. Moreover, other than isoconversional methods expect the value of the effective activation energy to remain constant throughput the glass transition. In order to determine thus an average effective activation energy ΔE_{ave} Moynihan et al. [30] have proposed the use of a dependence of the T_g on the rate of heating or cooling in accord with Eq. (1) as

$$\frac{\Delta E_{ave}}{R} = \frac{\mathrm{d}(\ln|\beta|)}{\mathrm{d}(1/T_g)} \quad (3)$$

For heating, Eq. (3) is applicable subject to the constraint that prior to heating the glassy material should be cooled from above to well below the glass transition region at a rate whose absolute value is equal to the rate of heating.

From Fig. 2 the glass transition temperatures measured at different heating rates where 119.8, 120.8, 121.6, 122.5, 123.5 and 124.2 °C for the heating rates 5, 7.5, 10, 15, 20 and 25 °C/min, respectively. From these values and Eq. (3) the average effective activation energy was estimated using either the 5–25 °C/min heating rate range or the 10–25 °C/min. The resulted values were 477 and 451 kJ/mol, respectively and are plotted as straight lines in Fig. 4. These follow the corresponding values estimated from the isoconversional methods.

The ΔE_x dependencies can be further converted to the dependencies of ΔE_x on T. This is accomplished by replacing X with an average of the temperatures corresponding to this X at different heating rates [42,43]. The resulting temperature dependencies are presented in Fig. 5. The values of ΔE_x in the 10–25 °C/min region decrease from 590 to 430 kJ/mol, which is in the same order of magnitude with those reported earlier by Vyazovkin et al. (i.e. 510 to 370 kJ/mol) [42,43].

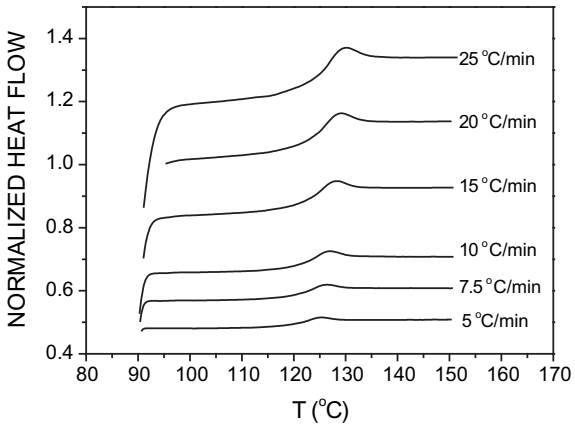

Fig. 1. DSC curves of PEN glass transition temperature at different heating rates.

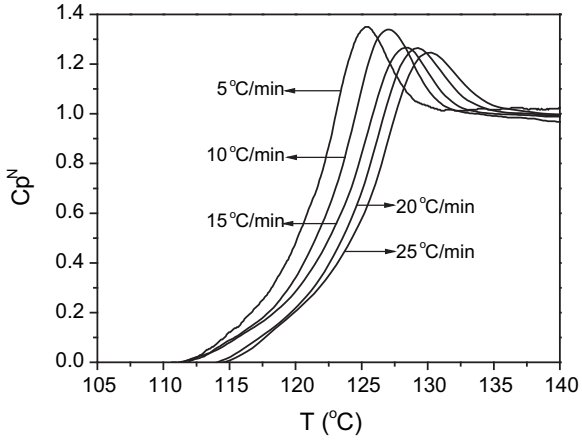

Fig. 2. Temperature dependence of the normalized heat capacity determined for PEN at different heating rates.

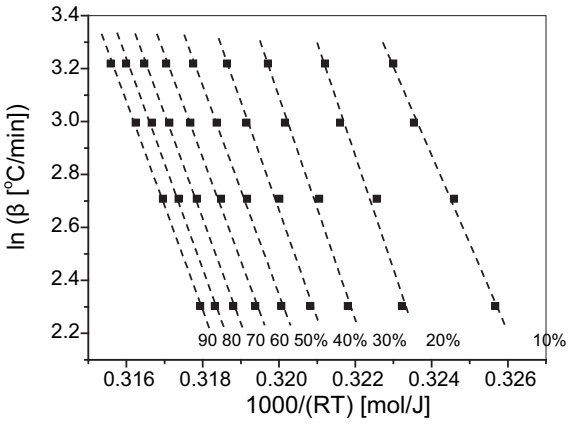

Fig. 3. Typical plots of $\ln(\beta)$ vs $1000/(RT)$ at different Xs.

Finally, it has been proposed that the observed decrease of ΔE_x with T could be consistent with the general tendency predicted by the WLF equation:

$$E = 2.303R\frac{C_1^0 C_2^0 T^2}{\left(C_2^0 + T - T_g\right)^2} \quad (4)$$

where, C_1^0 and C_2^0 are constants, which for temperatures at the vicinity of T_g take the universal WLF values 17.44 and 51.6 K, respectively.

By taking an average $T_g = 123\,^\circ$C, Eq. (4) can simulate the experimental data very well (Fig. 5) using the values 8.1 and 51.6 K for C_1^0 and C_2^0, respectively.

Moreover, Vyazovkin et al. [43], in order to correlate the effective activation energy with the dynamic fragility of a sample introduced a variability parameter, Δ_E, denoting the rate of change of ΔE_x with temperature and defined as

$$\Delta_E = \frac{\Delta E_{0.25} - \Delta E_{0.75}}{T_{0.25} - T_{0.75}} \quad (5)$$

where $\Delta E_{0.25}$ and $\Delta E_{0.75}$ are the effective activation energy values at $X = 0.25$ and 0.75 respectively and $T_{0.25}$ and $T_{0.75}$ are the values of T_x for the respective values of X. Then from the values reported in Fig. 5, the variability parameter for PEN was estimated to be equal to −15.6 kJ/mol/K, close to that reported by Vyazovkin et al. (i.e. −10 kJ/mol K) [43].

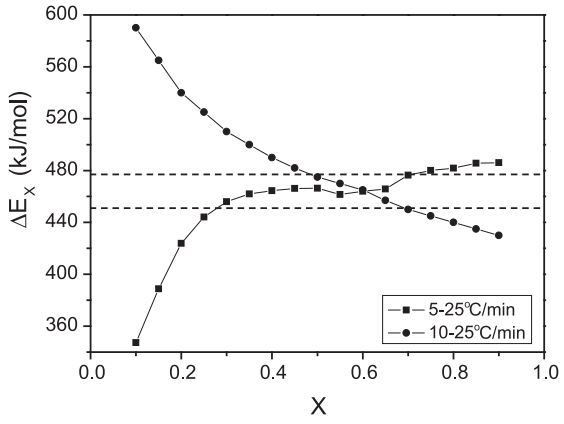

Fig. 4. Variation in the effective activation energy with the extent of conversion from the glassy to the liquid state for PEN at two different heating-rate ranges (i.e. 5–25 °C/min and 10–25 °C/min). Straight lines represent the constant values estimated from Eq. (3).

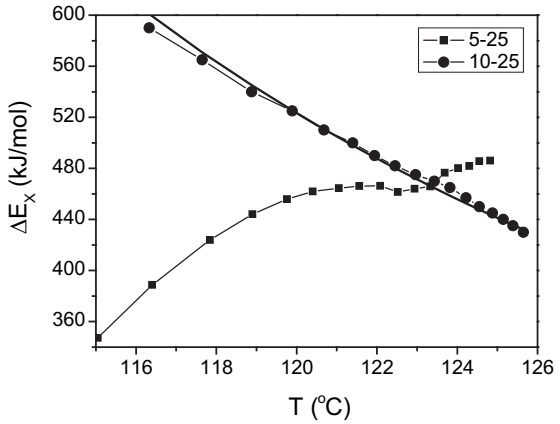

Fig. 5. Variation in the effective activation energy with temperature for PEN at two different heating-rate ranges (i.e. 5–25 °C/min and 10–25 °C/min). The straight line represents the values estimated from Eq. (4).

3.2. Prediction of PEN dynamic fragility

In this section the dynamic fragility of PEN was estimated using two thermal methods reviewed in the paper of Crowley and Zografi [51].

3.2.1. Calculation using the scanning rate dependency of T_g

At a single temperature, the fragility parameter, m could be defined by [51]:

$$m \equiv \left.\frac{\mathrm{d}\log\tau}{\mathrm{d}(T_g/T)}\right|_{T=T_g} = \frac{\Delta E_{T_g}}{(\ln 10)RT_g} \quad (6)$$

where τ is a mean relaxation time given by the following form of the Vogel–Tammann–Fulcher (VTF) equation:

$$\tau = \tau_0 \exp\left(\frac{DT_0}{T - T_0}\right) \quad (7)$$

τ_0, D and T_0 are constants, with D termed the strength parameter, with a large value (>30) representing 'strong' behavior and low D value (<10) representing 'fragile' behavior. According to the assumptions made in Ref. [51], parameter D can be calculated by the following Eq. (8) using $m_{\min} = 16$

$$D = \frac{(\ln 10)m_{\min}^2}{m - m_{\min}} \quad (8)$$

In Eq. (6), ΔE_{T_g} is equal to the average effective activation energy, ΔE_{ave} calculated from the variation of T_g with the heating rate, Eq. (3). Therefore, using the value estimated in the previous section, i.e. $\Delta E_{T_g} = 451$ or 477 kJ/mol, m is calculated from Eq. (6) to be equal to 60 or 63, respectively. These values are similar to that reported in Ref. [43] taken from Ref. [52] (i.e. 66). A large m value indicates rapidly changing dynamics at T_g which equates to 'fragile' behavior. Parameter D is then calculated form Eq. (8) to be equal to 13.5 or 12.5, respectively.

3.2.2. Extrapolation of configurational entropy to zero

According to this procedure, the fragility, m, is determined from Eq. (9), which results from substitution of the VTF Eq. (7), into Eq. (6).

$$m = \frac{DT_0/T_g}{\left(\ln 10\right)\left(1 - T_0/T_g\right)^2} \quad (9)$$

For the estimation of T_0 the assumption made is that it is equal to the Kauzmann temperature, T_K that describes the isoentropic point

between a super-cooled liquid and crystal. Taking the extrapolation of the configurational entropy to zero, allows estimation of T_K from the following relationship:

$$\frac{1}{T_K} = \frac{1}{T_m}\left(1 + \frac{\Delta H_m}{C_p^{conf} T_g}\right) \quad (10)$$

where, ΔH_m represents the enthalpy of melting and C_p^{conf} is the configurational C_p. C_p^{conf} is calculated from the difference in C_p between the amorphous and the crystalline phase at temperature equal to T_g. Then from the ATHAS data bank, for PEN [53] it is calculated as: $C_p^{conf} = C_p^{amorph} - C_p^{cryst}|_{T=T_g} = 428 - 343.3 = 84.7$ J/mol/K.

The strength parameter, D is estimated using the VTF Eq. (7) at $T = T_g$, $T_0 = T_K$, τ at T_g approximately equal to 10^2 s (which has been found from thermal analysis at a heating rate of 10 K/min) and τ_0 representing the timescale of vibrational motions, approximately equal to 10^{-14} s [51].

In this investigation, two values were assumed for ΔH_m, i.e. either 25 kJ/mol, taken from the work of Cheng and Wunderlich [53,54], or 46 kJ/mol estimated from the 190 J/g value given in the work of Zachmann and co-workers [5]. T_g was set equal to the glass transition temperature onset, i.e. 390 K. Results for m and D were calculated with also two values for T_m, the first (i.e. 333.5 °C) representing the equilibrium melting point, as it is estimated in the next paragraph and the other the typical melting point of PEN, i.e. 267 °C. The values of m and D are illustrated in Table 1. The $m = 145$ is exactly the same with that estimated in ref. [55], while $D = 5$ is near that reported in Ref. [56] (i.e. 5.6). Moreover, the value near 13 obtained for D in the previous section, lies in between the two limits reported in Table 1 (i.e 5 and 20).

Furthermore, the variation of the relaxation time, τ with temperature according to the VTF Eq. (7) appears in Fig. 6 for two values of the parameter D. As it can be seen, using the value of $D = 5$ the shape of the curve represents a more fragile material, while using the value of 20 for D the shape of the curve denotes a more strong material.

3.3. Isothermal crystallization

Following, the isothermal crystallization of PEN was investigated in a series of experiments, according to the self-nucleation procedure similar to that proposed by Müller et al. [46,47] and described in the experimental section. The temperatures where tests were conducted ranged from 210 to 260 °C with intervals of 2.5 °C. The subsequent heating scans after isothermal crystallizations are exhibited in Fig. 7. As can be seen in the heating scans multiple melting peaks appear if crystallization occurrs below 240 °C. Multiple melting behavior of PEN was analyzed in a few papers in the past and in general it was attributed to partial melting recrystallization and final melting of the recrystallized material [18,19,54]. Single melting peaks appear only in the heating scans after crystallization at T_cs equal or above 250 °C. Then peak temperature increases with increasing crystallization temperature.

Table 1
Fragility, m from Eq. (9), parameter D from Eq. (7) and T_K from Eq. (10) estimated at different values of ΔH_m and T_m.

ΔH_m (kJ/mol)	T_m^o (°C)	T_K (K)	D	m
25[a]	333.5	345.0	5	145
25[a]	267.0	307.5	10	76
46[b]	333.5	253.6	20	46

[a] Value reported by Cheng and Wunderlich [53,54].
[b] Value reported by Zachmann and co-workers [5].

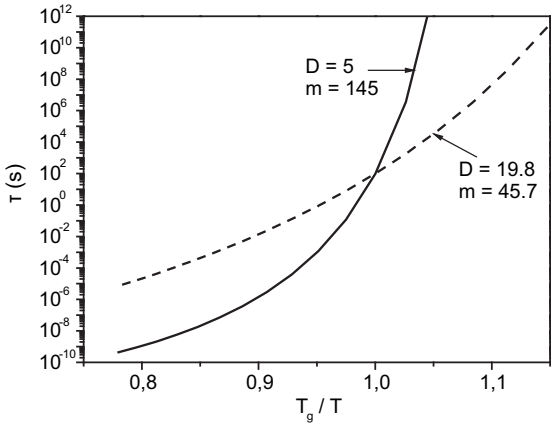

Fig. 6. Relaxation time versus temperature scaled to T_g at two sets of the D, m parameters. Notice that a large value for D (>30) represents a 'strong' behavior, while a low D value (<10) represents 'fragile' behavior.

These temperatures were used to estimate the equilibrium melting temperature of PEN.

3.3.1. Determination of the equilibrium melting temperature

Equilibrium melting temperature (T_m^o) is one the most important parameters characterizing a polymer. Study of crystallization of polymers demands knowledge of T_m^o which by definition is the melting temperature of lamellar crystals with an infinite thickness. Extrapolative methods are used to estimate equilibrium melting temperature (T_m^o). The Hoffman–Weeks (H–W) method has been commonly used and accepted to estimate T_m^o [57]. In this procedure, the measured T_ms of specimens crystallized at different crystallization temperatures (T_cs) are plotted against T_c and a linear extrapolation to the line $T_m = T_c$, and the intercept gives T_m^o. In the Hoffman–Weeks equation:

$$T_m = T_m^o\left(1 - \frac{1}{r}\right) + \frac{T_c}{r} \quad (11)$$

T_m is the observed melting temperature of a crystal formed at a temperature T_c, r is the thickening coefficient equal to l_c/l_g^* where l_c is the thickness of the grown crystal and l_g^* is the initial thickness of a chain-folded lamellar crystal [57]. The prerequisite for the application of this theory is the isothermal thickening process of

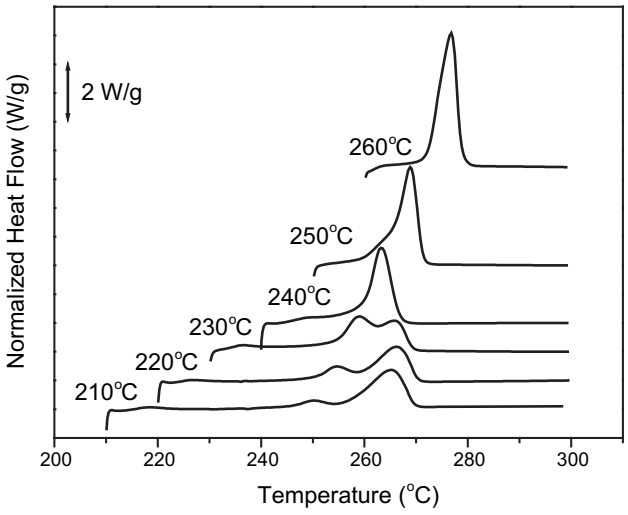

Fig. 7. DSC heating scans of PEN samples isothermally crystallized at different temperatures.

lamellar crystals at a specific crystallization temperature and the dependence of the thickening coefficient on the crystallization temperature.

In this work the Hoffman–Weeks extrapolation was used for the estimation of T_m^os of PEN. The respective plot is shown in Fig. 8. The obtained T_m^o value was 333.5 °C. This value is close to that reported by Chen and Wunderlich (337 °C) [54], while higher than that reported by Woo et al. (289 °C) [18], Lee and Cakmak (296 °C) [17], etc.

3.3.2. Secondary nucleation theory

It has been suggested that the kinetic data of isothermal polymer crystallization can be analyzed using the spherulitic growth rate in the context of the Lauritzen–Hoffman secondary nucleation theory [58,59]. Accordingly, the growth rate G is given as a function of the crystallization temperature, T_c by the following bi-exponential equation:

$$G = G_0 \exp\left[-\frac{U^*}{R(T_c - T_\infty)}\right]\exp\left[-\frac{K_g}{T_c(\Delta T)f}\right] \quad (12)$$

where, G_0 is the pre-exponential factor, the first exponential term contains the contribution of diffusion process to the growth rate, while the second exponential term is the contribution of the nucleation process; U^* denotes the activation energy which characterizes molecular diffusion across the interfacial boundary between melt and crystals, usually set equal to 1500 cal/mol (6285 J/mol) and T_∞ is the temperature below which diffusion stops, usually equal to $T_\infty = T_g - 30$ K; K_g is a nucleation constant and ΔT denotes the degree of undercooling ($\Delta T = T_m^0 - T_c$); f is a correction factor which is close to unity at high temperatures and is given as $f = 2T_c/(T_m^0 + T_c)$; the equilibrium melting temperature, T_m^0 was set equal to 333.5 °C, finally the glass transition temperature was assumed equal to 123 °C. The nucleation parameter, K_g, is usually calculated from Eq. (12) using the double logarithmic transformation:

$$\ln(G) + \frac{U^*}{R(T_c - T_\infty)} = \ln(G_0) - \frac{K_g}{T_c(\Delta T)f} \quad (13)$$

Plotting the left-hand side of Eq. (13) with respect to $1/(T_c(\Delta T)f)$ a straight line should appear having a slope equal to K_g. Critical break points, identified by the change in the slope of the line, when appear in such a plot, have been attributed to regime transitions accompanied by morphological changes of the crystals formed (i.e. change from axialite-like to banded spherulite and non-banded spherulite morphology).

Morphology and sperulitic growth rates were studied using PLM. Referring to the generated morphologies during isothermal crystallization of PEN elliptical-shaped hedrite-like morphology appeared at temperatures equal or higher than 253 °C. In general PEN showed fast nucleation rates and small spherulites, especially below 243 °C. These observations are obviously close related with the crystallization regimes. Regime I is supposed to hold at high temperatures where growth rates are much faster compared to nucleation rates. Regime II holds when growth and nucleation rates are comparable, while in regime III which is expected at low crystallization temperatures, nucleation is much faster than crystal growth. Results for growth rates from PLM measurements appear in Fig. 9. Growth rates decrease with increasing crystallization temperature. As a matter of fact in the Lauritzen–Hoffman type plot (Fig. 10) two break points appear, the one corresponding to regime II to regime I transition at about 253 °C and the second at about 243 °C for regime III to regime II transition. The K_g values estimated, were 8.37×10^5, 4.2×10^5 and $8.35 \times 10^5 K^2$ for regimes I, II and III, respectively and they are summarized in Table 2. As can be seen, for regime I and III, K_g is about 8.4 and for regime II, 4.2 that is the ratios K_{gIII}/K_{gII} and K_{gI}/K_{gII} are very close to the expected value 2. Also such high K_g values are consistent with the significant rigidity of the macromolecular chains of PEN due to the presence of the naphthalene ring. In this work regime transitions were found to occur at high temperatures. In contrast Lee et al. [37] reported a regime II to regime I transition at about 230 °C which is rather too low. In fact there was a skepticism about the applicability of the secondary nucleation theory in case of semirigid chain polymers like PEN [60]. A regime II to regime I transition above 250 °C was also supposed by Lee and Cakmak, although their conclusions were based on growth rates measurements at limited temperatures [17].

For a secondary or heterogeneous nucleation, K_g can be calculated from:

$$K_g = \frac{n\sigma\sigma_e b_0 T_m^0}{\Delta h_f \rho_c k_B} \quad (14)$$

where, n is a constant equal to 4 for regime I and III and 2 for regime II, σ, σ_e are the side surface (lateral) and fold surface (end) free energies which measure the work required to create a new surface, b_0 is the single layer thickness, $\Delta h_f\ \rho_c = \Delta H_f$ is the enthalpy of melting per unit volume and k_B is the Boltzmann constant ($k_B = 1.38 \times 10^{-23}$ J/K).

In order to estimate the parameters appearing in Eq. (14), the values proposed by Lee et al. [37] and the assumptions made there,

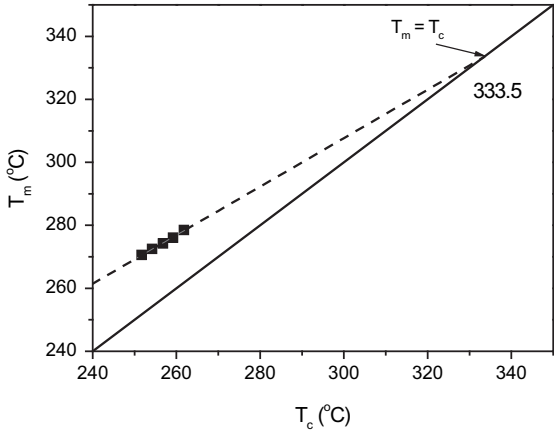

Fig. 8. Hoffman–Weeks type plot to estimate the equilibrium melting point.

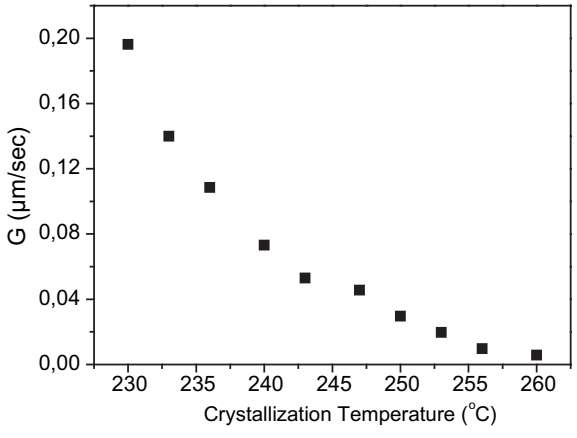

Fig. 9. Variation of growth rate with crystallization temperature obtained from PLM measurements.

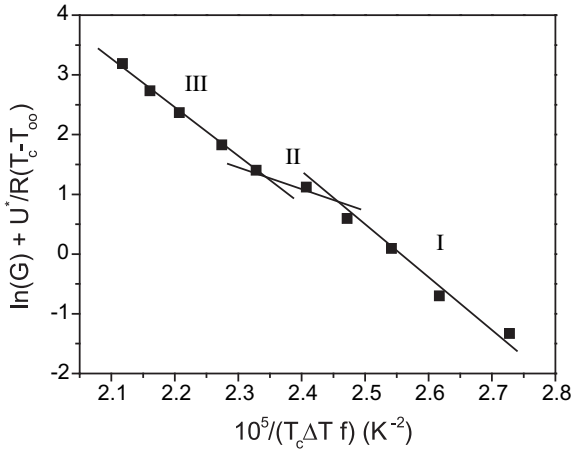

Fig. 10. Lauritzen–Hoffman type plot obtained from PLM measurements and exhibiting regime transitions.

were adopted. Accordingly, since β-form crystals are assumed to grow at the regime I region and α-form in regime II region, different input parameters for the calculation of the surface free energy $\sigma\sigma_e$ were used. According to the X-ray studies of Zachmann et al. and others [5,18] crystallization from the melt usually results in formation of crystals of both crystal modifications of PEN, although at temperatures above 240 °C it mainly produces crystals of β-modification and the opposite is supposed to occur at lower temperatures. In this work, during PLM study above 253 °C hedrites (or spherulites with squeezed peanut shape) were observed, although usual spherulites were still present. Hedrites are supposed to be formed by crystals of β-modification, while spherulites are formed by crystals of α-modification [37]. It must be noted here that at temperatures above 253 °C growth rates of hedrites were measured. In contrast, at lower temperatures growth rates of spherulites were measured. Thus, in computations using PLM data for regime I that is for temperatures above 253 °C, the parameters associated with the unit cell of crystal of β-modification were used, while for regime II and III the parameters of the unit cell of crystal of α-modification were supposed. In case of DSC data, the samples were first self-nucleated before isothermal crystallization. Thus, the procedure involved crystallization at 210 °C first, which is related with formation of crystals of α-modification mainly and then melting and self nucleation at 275 °C, which means that nuclei of crystals of α-modification were remained and thus formation of crystals of α-modification is expected during isothermal crystallization at least at low temperatures. Formation of crystals of β-modification can still occur in this case during isothermal crystallization at temperatures above 240 °C. Thus, the same methodology as for the treatment of PLM data was followed. Differences however may be due to the fact that at regime I it is not so sure that overall growth rates are related with growth of crystals of β-modification. The monomolecular layer thickness, b_0 value, of the α-form was taken as the *d*-spacing of the (010) plane, while b_0 of the β-form was taken as the *d*-spacing of the (020) plane. On the other hand, the lateral surface free energy, σ is commonly estimated as [58]:

$$\sigma = \alpha\left(\Delta h_f\right)(a_0 b_0)^{0.5} \tag{15}$$

where, α was derived empirically to be 0.11 by analogy with the well-known behavior of hydrocarbons. a_0 and b_0 factors are the monomolecular width and layer thickness, respectively. The input data and the results obtained from the secondary nucleation analysis are listed in Table 2.

Finally, the work of chain folding, *q*, which is most closely correlated with molecular structure, can be calculated from:

$$q = 2a_0 b_0 \sigma_e \tag{16}$$

The values of *q* are also illustrated in Table 2. The work of chain folding calculated for PEN was higher than that for PBN [61], meaning that the inherent stiffness of the PEN chains is larger than that of the PBN chains.

Instead of using PLM measurements, several authors have treated the isothermal crystallization rate data obtained by DSC, according to the Lauritzen–Hoffman analysis (Eq. (7)) [62–66]. The basic assumption used for the evaluation of *G* was that the spherulite growth rate is inversely proportional to the crystallization half-time, $G \approx 1/t_{1/2}$ [62]. This approximation although it is purely empirical has been widely used in literature [61–70] to evaluate the nucleation parameter K_g. Muller and co-workers [46] proposed a self-nucleation procedure for isothermal crystallization to better approximate crystal growth rates, by neglecting nucleation. Then the resulting $1/t_{1/2}$ values can be used in the L–H analysis. This method was also used in this work.

In order to estimate $t_{1/2}$, the relative degree of crystallinity, *X*, is calculated from Eq. (17) based on the assumption that the evolution of crystallinity is linearly proportional to the evolution of heat released during the crystallization

$$X(t) = \frac{\int_0^t (dH_c/dt)dt}{\int_0^\infty (dH_c/dt)dt} \tag{17}$$

where dH_c denotes the measured enthalpy of crystallization during an infinitesimal time interval d*t*. The limits *t* and ∞ are used to denote the elapsed time during the course of crystallization and at the end of the crystallization process, respectively.

Results on the variation of the relative degree of crystallinity with time during isothermal crystallization of PEN at temperatures from 230 to 260 °C by 2.5 °C appear in Fig. 11. From these curves, the half time of crystallization, $t_{1/2}$, can be directly determined as the time elapsed from the onset of crystallization to the point where the crystallization is half completed.

Variation of $1/t_{1/2}$ with T_c appears in Fig. 12. From the data displayed in this figure it is apparent that the $t_{1/2}$ values increase almost exponentially as the crystallization temperature is increased, which means that the crystallization rates, denoted by $1/t_{1/2}$, decrease with increasing temperature. The Lauritzen–Hoffman-type plot constructed using the $1/t_{1/2}$ values in the place of *G*, appear in Fig. 13. As it can be seen, two break points corresponding to regime II to regime I transition at about 252–255 °C and regime

Table 2
Kinetic data for crystallized PEN calculated from secondary nucleation theory and PLM measurements.

	Regime I	Regime II
K_g (K^2)	8.37×10^5	4.20×10^5
U^* (J/mol)	6285	6285
$\sigma\sigma_e$ ($(J\,m^{-2})^2$)	2.72×10^{-3}	2.26×10^{-3}
σ ($J\,m^{-2}$)	14.1×10^{-3}	17.8×10^{-3}
σ_e ($J\,m^{-2}$)	193×10^{-3}	127×10^{-3}
q ($kJ\,mol^{-1}$)	51.5	56.4
Parameters of input data from ref. [37]		
n	4	2
a_0 (nm)	0.463	0.651
b_0 (nm)	0.478	0.566
$\Delta h_f \times 10^6$ ($J\,m^{-3}$)	273.4	267.3

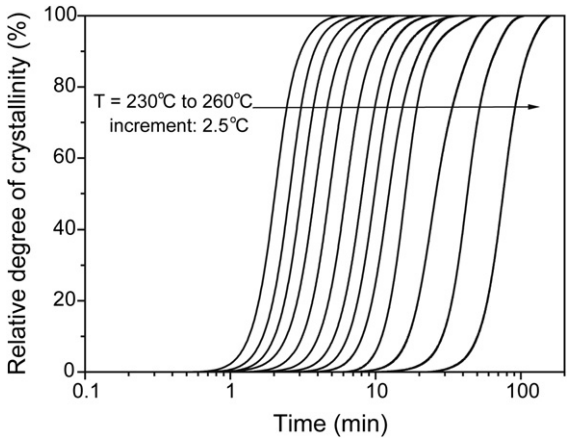

Fig. 11. Relative degree of crystallinity versus time during isothermal crystallization of PEN at different temperatures.

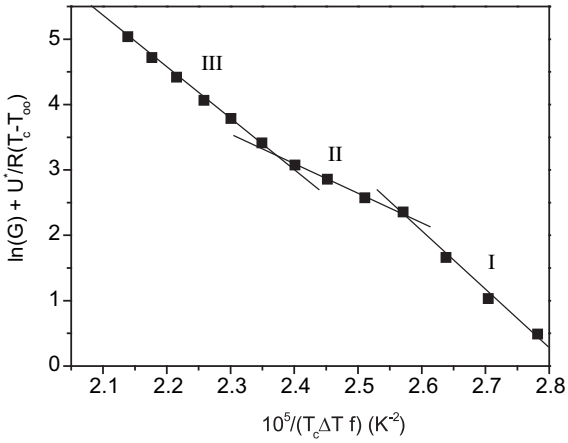

Fig. 13. Lauritzen–Hofmann type plot obtained from DSC measurements with $G = 1/t_{1/2}$ and exhibiting regime transitions.

III to regime II transition at about 245 °C, appear. These temperatures are essentially the same with those found using PLM data, as was describe above. The K_g value for regime I was found here about $8.2 \times 10^5 K^2$, very close to $8.4 \times 10^5 K^2$ found using PLM data, while for regime II was $4.3 \times 10^5 K^2$ well compared to the value $4.2 \times 10^5 K^2$ found using PLM data (Table 3). For regime III, K_g was estimated to be $7.7 \times 10^5 K^2$, close to the respective value $8.4 \times 10^5 K^2$ found using PLM data. The ratios K_{gIII}/K_{gII} and K_{gI}/K_{gII} in this case were found to be 1.80 and 1.92, respectively, very close to the theoretical value 2. Thus, the conclusion is that using the self-nucleation procedure for isothermal crystallization study with DSC gives very realistic results. In contrast, in most cases when DSC data are used without self-nucleation, then much larger K_g values are obtained compared to those from PLM measurements.

3.4. Isoconversional analysis of combined melt and cold crystallization data

In this section, several crystallization experiments were carried out under non-isothermal conditions either on cooling (melt crystallization) or heating (cold crystallization). The aim was to combine both crystallization rates into one set and fit it to the Lauritzen–Hoffman equation according to a methodology proposed by Vyazovkin and Dranca [71].

According to Vyazovkin and Sbirrazzuoli [72,73] the most attractive feature in applying the isoconversional methods to DSC data is that the resulting ΔE_x dependencies can be utilized for estimating the parameters of the Lauritzen–Hoffman theory.

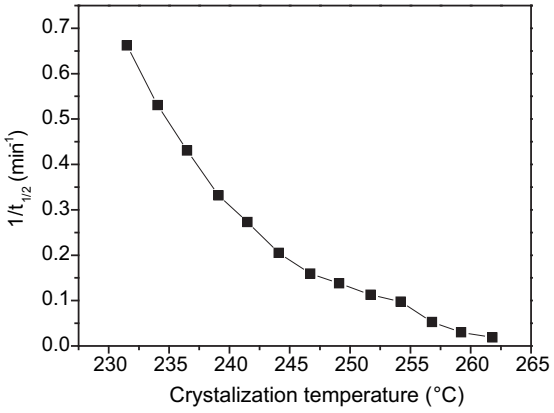

Fig. 12. Variation of $1/t_{1/2}$ with crystallization temperature obtained from isothermal DSC experiments.

Extensive experimental measurements by Toda et al. [74] demonstrate that the logarithmic derivative of the microscopic growth rate is equivalent to the logarithmic derivative of the overall crystallization rate, Φ, according to:

$$\frac{\mathrm{d}\ln(G)}{\mathrm{d}T^{-1}} = \frac{\mathrm{d}\ln(\Phi)}{\mathrm{d}T^{-1}} \tag{18}$$

where, G is the growth rate and $\Phi = \Delta h S G$ with Δh the volumetric heat of crystallization and S the total area of the growth surface.

Eq. (18) has been used by Vyazovkin and Sbirrazzuoli [72,73] together with Eq. (12) to derive the temperature dependence of the effective activation energy of the growth rate as follows:

$$\Delta E = -R\frac{\mathrm{d}(\ln G)}{\mathrm{d}(1/T)} = U^*\frac{T^2}{(T-T_\infty)^2} + K_g R\frac{\left(T_m^0\right)^2 - T^2 - T_m^0 T}{\left(T_m^0 - T\right)^2 T} \tag{19}$$

The validity of Eq. (19) has been recently tested by Achilias et al. [61] using different polymers. This temperature dependence of the effective activation energy can be relatively easy obtained by applying certain isoconversional methods to DSC data. Several mathematical procedures have been proposed in literature for the calculation of effective activation energy of non-isothermal crystallization, such as the differential isoconversional method of Friedman and the advanced integral isoconversional method of Vyazovkin and Sbirrazzuoli [72]. In this investigation the method of Friedman was used. According to the differential isoconversional method of Friedman, different effective activation energies are calculated for every degree of crystallinity from:

$$\ln\left(\frac{\mathrm{d}X}{\mathrm{d}t}\right)_{X,i} = \mathrm{Const} - \frac{\Delta E_X}{RT_{X,i}} \tag{20}$$

where $\mathrm{d}X/\mathrm{d}t$ is the instantaneous crystallization rate as a function of time at a given conversion X, ΔE_x is the effective activation

Table 3
Kinetic data for crystallized PEN calculated from secondary nucleation theory and DSC measurements.

	Regime I	Regime II
K_g (K^2)	8.18×10^5	4.27×10^5
U^* (J/mol)	6285	6285
$\sigma\sigma_e$ ($(J\,m^{-2})^2$)	2.66×10^{-3}	2.29×10^{-3}
σ ($J\,m^{-2}$)	14.1×10^{-3}	17.8×10^{-3}
σ_e ($J\,m^{-2}$)	189×10^{-3}	129×10^{-3}
q ($kJ\,mol^{-1}$)	50.4	57.3

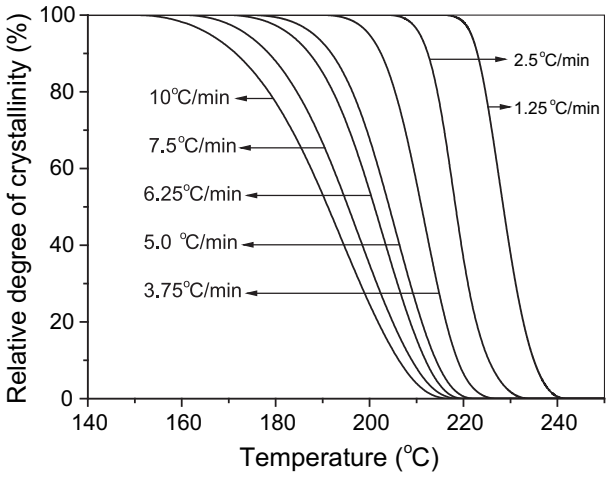

Fig. 14. Relative degree of crystallinity versus temperature during non-isothermal melt crystallization of PEN at different cooling rates.

energy at a given conversion X, $T_{x,i}$ is the set of temperatures related to a given conversion X at different cooling rates, β_i and the subscript i refers to every individual cooling rate used.

According to this method, the $X(t)$ function obtained from the integration of the experimentally measured crystallization rates is initially differentiated with respect to time to obtain the instantaneous crystallization rate, dX/dt. Furthermore, by selecting appropriate degrees of crystallinity (i.e. from 5% to 95%) the values of dX/dt at a specific X are correlated to the corresponding crystallization temperature at this X, i.e. T_x. Then by plotting the left hand side of Eq. (20) with respect to $1/T_x$ a straight line must be obtained with a slope equal to $\Delta E_x/R$. The ΔE_x dependence on T needed for evaluating the Lauritzen–Hoffman parameters K_g and U^* in Eq. (19) is readily obtained by replacing X with the temperature which is estimated as an average of the temperatures corresponding to this X at different heating or cooling rates.

Results on the relative degree of crystallinity as a function of temperature obtained from melt crystallization experiments of PEN at different cooling rates appear in Fig. 14. Application of the differential isoconversional method, Eq. (20), at different Xs from 0.1 to 0.9 to estimate the effective activation energy, linear curves were obtained for cooling rates ranging between 2.5 and 10 °C/min. The effective activation energy, thus obtained, was subsequently plotted as a function of the relative degree of crystallinity, as one can see in Fig. 15. The effective activation energy increases with X as

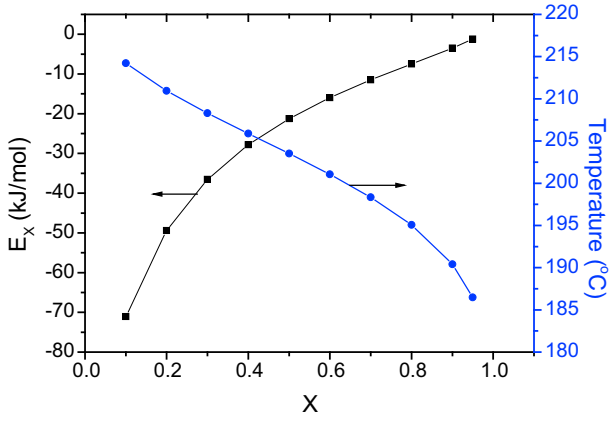

Fig. 15. Effective activation energy (squares) and average temperature corresponding to various extents of relative crystallization (circles) as a function of the relative extent of crystallization for melt crystallization of PEN.

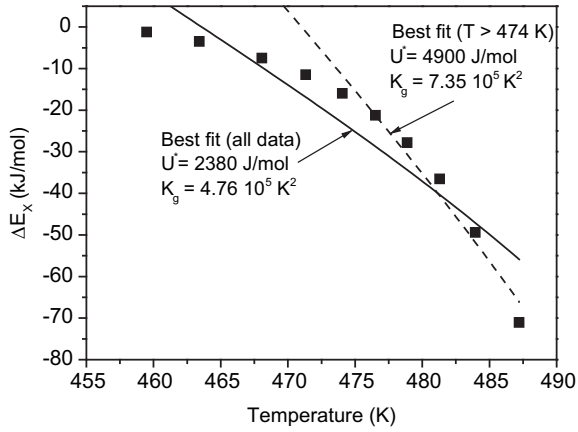

Fig. 16. Effective activation energy as a function of temperature for melt crystallization of PEN. Lines represent results of the non-linear fitting procedure using Eq. (19).

it has also been observed in other systems. As described previously, the ΔE_x dependence can be converted into a ΔE versus T dependence if an average temperature for the corresponding X is evaluated. This plot is presented in Fig. 16. As it was expected a decrease of the effective activation energy with temperature was observed. Using Eq. (19) and the Marquardt–Levenberg non-linear optimization algorithm the best fit values of U^* and K_g estimated with all experimental data points were 2376 J/mol and $4.76 \times 10^5 K^2$, respectively. Since the value of U^* was rather low, we also used the same equation but only data points above 474 K to find new best fit values of the L–H parameters. The new estimated values for U^* and K_g were 4905 J/mol and $7.35 \times 10^5 K^2$, respectively. According to the temperature range, regime III was assumed following the values reported in a previous section. Then, the estimated K_g is very close to the value found with the DSC measurements (i.e. $7.69 \times 10^5 K^2$), while the U^* was much lower.

As a step further, the differential isoconversional method was applied to the cold crystallization data and the dependence of the effective activation energy with the relative degree of crystallinity appear in Fig. 17. Again, as expected from the theory [71] the dependence is decreasing. However, since this time the values were estimated from heating experiments, all ΔE_x have positive sign. Finally the respective ΔE_x versus T dependence is shown in Fig. 18. In the same figure the results from the melt crystallization have been included also. It was very interesting that the part of the two different experimental data were simulated by the same line

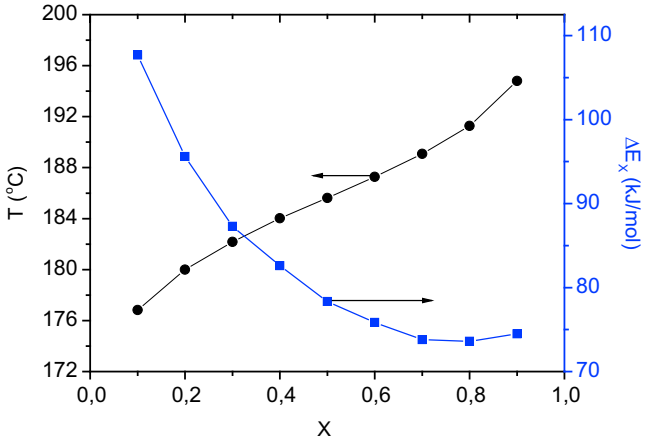

Fig. 17. Effective activation energy (squares) and average temperature corresponding to various extents of relative crystallization (circles) as a function of the relative extent of crystallization for cold crystallization of PEN.

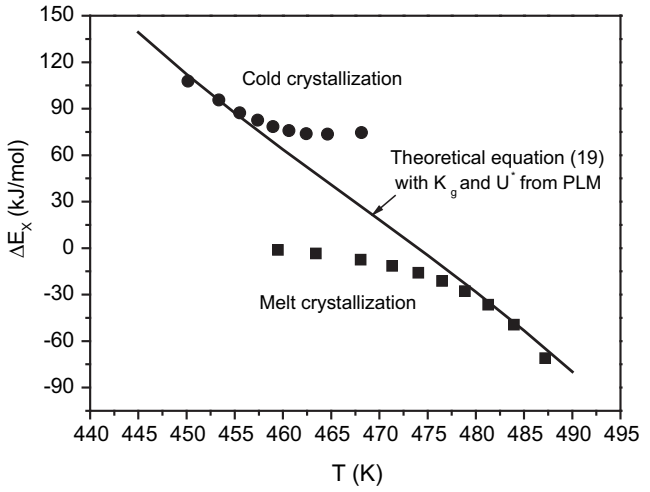

Fig. 18. Experimental effective activation energy versus T data for melt (squares) and cold (circles) crystallization of PEN. Solid line represents results of Eq. (19) using the K_g and U^* values from PLM measurements (regime III).

coming from Eq. (19) with the K_g and U^* values estimated from PLM measurements in regime III (see Table 2). Therefore, it seems that Eq. (19) is valid in both crystallization experiments.

4. Conclusions

Isoconversional methods were applied to DSC data to determine the effective activation energy for the glass transition in PEN. A decrease with temperature was observed. Using the same data and different thermal methods, the dynamic fragility of PEN was also evaluated.

Secondary nucleation theory was used for the analysis of the spherulitic growth rates during isothermal crystallization of the polymer. Using PLM measurements, the Lauritzen–Hoffmann type plots showed two critical break points, at about 253 °C and 243 °C, being attributed to regime II to I and III to II transitions, respectively. The nucleation constant K_g for regime I and III was about $8.4 \times 10^5 K^2$ while for regime II $4.2 \times 10^5 K^2$ that is the ratios K_{gIII}/K_{gII} and K_{gI}/K_{gII} were very close to the expected value 2. Such high K_g values are consistent with the significant rigidity of the macromolecular chains of PEN due to the presence of the naphthalene ring. Above 253 °C elliptical-shaped hedrite-like morphology was observed, while at lower temperatures only spherulites appeared. Below 243 °C the nucleation rates of PEN were very fast.

The same procedure to estimate the Lauritzen–Hoffman parameters was followed but using DSC data from self nucleation experiments and the inverse of crystallization half times in place of the growth rate. Break points were observed at 255 °C and 245 °C for regime II to regime I and regime III to regime II, transitions, respectively. The K_g values were found to be similar to those from the PLM measurements (i.e. about 8.2×10^5, 4.3×10^5 and $7.7 \times 10^5 K^2$, for regime I, II and III, respectively). The ratios K_{gIII}/K_{gII} and K_{gI}/K_{gII} were about 1.90. It was thus verified that using the DSC self-nucleation experiments, the effect of nucleation is neglected and the measured values are related directly with crystal growth.

In the DSC heating scans after isothermal crystallization above 253 °C single melting peaks appear, while double peaks appear in the respective traces for samples crystallized at temperatures in between 243 °C and 253 °C and finally triple melting behavior is observed for samples crystallized below 243 °C. These observations are evidences for the regime transitions, since they obviously have to do with the relative rates of nucleation and crystal growth.

Finally, the effective activation energy was calculated using the isoconversional method of Friedman for both melt and glass non-isothermal crystallization. The combined set of activation energies was found to be described by the theoretical Vyazovkin–Sbirrazzuoli equation using a single set of LH parameters coming from PLM measurements.

References

[1] Ghahem AM, Porter RS. J Polym Sci Polym Phys Ed 1989;17:480.
[2] Karayannidis GP, Papageorgiou GZ, Bikiaris DN, Tourasanidis EV. Polymer 1998;39:4129.
[3] Garcia Gutierrez MC, Rueda DR, Balta Calleja FJ, Stribeck N, Bayer RK. Polymer 2003;44:451.
[4] Garcia Gutierrez MC, Karger-Kocsis J, Riekel C. Macromolecules 2002;35:7320.
[5] Buchner S, Wiswe D, Zachmann HG. Polymer 1989;30:480.
[6] Widen H, Hall G. LWT 2007;40:66.
[7] Liu RYF, Schiraldi DA, Hiltner A, Baer E. J Polym Sci Part B Polym Phys 2002;40:862.
[8] McGonigle E-A, Liggat JJ, Pethrick RA, Jenkins SD, Daly JH, Hayward D. Polymer 2001;42:2413.
[9] Lachmann K, Eckert S, Vogel A, Klinger A, Gebert A, Klages C-P. Prog Org Coat 2009;64:294.
[10] Weick BL. J Appl Polym Sci 2009;111:899.
[11] Mills CA, Fernandez JG, Errachid A, Samitier J. Microelectron Eng 2008;85:1897.
[12] Laskarakis A, Logothetidis S. J Appl Phys 2007;101:053503.
[13] Ikegami M, Suzuki J, Teshima K, Kawaraya M, Miyasaka T. Solar Energy Mater Solar Cells 2009;93:836.
[14] Yoon WJ, Myung HS, Kim BC, Im SS. Polymer 2000;41:4933.
[15] Schoukens G, Verschuere M. Polymer 1999;40:3753.
[16] Gao X, Jin M, Bu H. J Polym Sci Part B Polym Phys 2000;38:3285.
[17] Lee SW, Cakmak M. J Macromol Sci Phys 1998;B37(4):501.
[18] Woo E, Huang D-H, Wu M- C. Macromol Chem Phys 2004;205:1644.
[19] Papageorgiou GZ, Karayannidis GP. Polymer 1999;40:5325.
[20] Hu YS, Rogunova M, Schiraldi DA, Hiltner A, Baer E. J Appl Polym Sci 2002;86:98.
[21] Nam JY, Fukuoka M, Saito H, Inoue T. Polymer 2007;48:2395.
[22] Etienne S, David L. Philos Mag 2007;87(3):417.
[23] Papageorgiou GZ, Karayannidis GP, Bikiaris DN, Stergiou A, Litsardakis G, Makridis SS. J Polym Sci Part B Polym Phys 2004;42:843.
[24] Gao X, Hou W, Zhou J, Li L, Zhao L. Macromol Mater Eng 2004;289:174.
[25] McGonigle E-A, Jenkins SD, Liggat JJ, Pethrick RA. Polym Int 2000;49:1458.
[26] Jeong YG, Jo WH, Lee SC. Polymer 2004;45:3321.
[27] Chen P, Kotek R. Polym Rev 2008;48(2):392.
[28] Robertson CG, Santangelo PG, Roland CM. J Non-Cryst Solids 2000;275:153.
[29] Angell CA, Ngai KL, McKenna GB, McMillan PF, Martin SW. J Appl Phys 2000;88:3113.
[30] Moynihan CT, Lee SK, Tatsumisago M, Minami T. Thermochim Acta 1996;280/281:153.
[31] Wang L-M, Velikov V, Angell CA. J Chem Phys 2002;117:10184.
[32] Chen K, Vyazovkin S. J Phys Chem B 2009;113:4631.
[33] Kim KH, Isayev AI, Kwon K. J Appl Polym Sci 2006;102:2847.
[34] Kim JY, Park HS, Kim SH. Polymer 2006;47:1379.
[35] Di Lorenzo ML. Prog Polym Sci 2003;28:663.
[36] Keller A, Hikosaka M, Rastogi S, Toda A, Barham PJ, Goldbeck-Wood G. J Mater Sci 1994;29:2579.
[37] Lee WD, Yoo ES, Im SS. Polymer 2003;44:6617.
[38] Di Lorenzo ML, Silvestre C. Prog Polym Sci 1999;24:917.
[39] Zheng L-J, Qi J-G, Zhang Q-H, Zhou W-F, Liu D. J Appl Polym Sci 2008;108:650.
[40] Kanuga K, Cakmak M. Polymer 2007;48:7176.
[41] Yoshioka T, Tsuji M, Kawahara Y, Kikutani T, Kohjiya S. Polymer 2005;46:1886.
[42] Vyazovkin S, Sbirrazzuoli N, Dranca I. Macromol Rapid Commun 2004;25:1708.
[43] Vyazovkin S, Sbirrazzuoli N, Dranca I. Macromol Chem Phys 2006;207:1126.
[44] Badrinarayanan P, Zheng W, Simon SL. Thermochim Acta 2008;468:87–93.
[45] Fillon B, Wittmann JC, Lotz B, Thierry A. J Polym Sci Part B Polym Phys 1993;31:1383.
[46] Müller AJ, Albuerne J, Marquez L, Raquez J-M, Degée P, Dubois P, et al. Faraday Discuss 2005;128:231.
[47] Boschetti-de-Fierro A, Lorenzo AT, Müller AJ, Schmalz H, Abetz V. Macromol Chem Phys 2008;209:476.
[48] Flynn H, Wall LA. J Res Natl Bur Stand 1966;70:587.
[49] Ozawa T. Bull Chem Soc Jpn 1965;38:1881.
[50] Badrinarayanan P, Simon SL, Lyng RJ, O'Reilly JM. Polymer 2008;49:3554–60.
[51] Crowley KJ, Zografi G. Thermochim Acta 2001;380:79–93.
[52] Nogales A, Denchev Z, Sics I, Ezquerra TA. Macromolecules 2000;33:9367.
[53] Pyda M. Advanced THermal analysis system. ATHAS data bank, available at: http://athas.prz.rzeszow.pl.
[54] Cheng SZD, Wunderlich B. Macromolecules 1988;21:789.

[55] Saiter A, Hess M, Saiter JM, Grenet J. Macromol Symp 2001;174:165–73.
[56] Sanz A, Nogales A, Ezquerra TA. Macromolecules 2010;43:29–32.
[57] Hoffman JD, Weeks JJ. J. Chem Phys 1965;42:4301.
[58] Hoffman JD, Davis GT, Lauritzen Jr JI. In: Hannay NB, editor. Treatise on solid state chemistry, vol. 3. New York: Plenum Press; 1976 [chapter 7].
[59] Hoffman JD, Miller RL. Polymer 1997;38:3151.
[60] Medellin-Rodriguez FJ, Phillips PJ, Lin JS. Macromolecules 1996;28:7744.
[61] Achilias DS, Papageorgiou GZ, Karayannidis GP. Macromol Chem Phys 2005;206:1511.
[62] Chan TW, Isayev AI. Polym Eng Sci 1994;34:461.
[63] Dangseeyun N, Shrimoaon P, Supaphol P, Nithitanakul M. Thermochim Acta 2004;409:63.
[64] Papageorgiou GZ, Achilias DS, Bikiaris DN, Karayannidis GP. Thermochim Acta 2005;427:117.
[65] Achilias DS, Papageorgiou GZ, Karayannidis GP. J Therm Anal Calorim 2006;86:791.
[66] Sorrentino L, Iannace S, Di Maio E, Acierno D. J Polym Sci Part B Polym Phys 2005;43:1966.
[67] Papageorgiou GZ, Bikiaris DN, Achilias DS. Thermochim Acta 2007;457:41.
[68] Papageorgiou GZ, Achilias DS, Bikiaris DN. Macromol Chem Phys 2007;208:1250.
[69] Papageorgiou GZ, Achilias DS, Bikiaris DN. Macromol Chem Phys 2009;210:90.
[70] Achilias DS, Papageorgiou GZ, Karayannidis GP. J Polym Sci Part B Polym Phys 2004;42:3775.
[71] Vyazovkin S, Dranca I. Macromol Chem Phys 2006;207:20.
[72] Vyazovkin S, Sbirrazzuoli N. Macromol Rapid Commun 2006;27:1515.
[73] Vyazovkin S, Sbirrazzuoli N. Macromol Rapid Commun 2004;25:733.
[74] Toda A, Oda T, Hikosaka M, Saruyama Y. Polymer 1997;38:233.